Applied Acoustics 116 (2017) 14–23

Contents lists available at ScienceDirect

Applied Acoustics

journal homepage: www.elsevier.com/locate/apacoust

Transfer matrix methods for sound attenuation in resonators with perforated intruding inlets

Rong Guo *, Wen-bo Tang

School of Automotive Studies, Tongji University, China
Clean Energy Automotive Engineering Center, Tongji University, China

ARTICLE INFO

Article history:
Received 19 July 2016
Received in revised form 7 September 2016
Accepted 9 September 2016

Keywords:
Perforated intruding inlet
Transfer matrix method
Transmission loss
Acoustic performance

ABSTRACT

A resonator with perforated intruding inlet (PII) is a superior silencer element, since the use of perforated inlet extensions can dramatically improve the acoustic performance. In this work, both a one-dimensional (1D) and a two-dimensional (2D) transfer matrix methods are developed to predict the transmission loss of the resonator without considering the mean flow. Based on the two groups of comparisons with tests, it is found out that the applicability of 1D method is limited by the resonator geometry even when the frequency is below the cut-off value of plane wave. Whereas the 2D approach is much more accurate while predicting the transmission losses within entire frequency range. Subsequently, five groups of resonators are chosen to determine the effects of structure parameters to transmission loss based on the 2D approach. The resonant frequency decreases and more resonant peaks appear when the length of inlet extension increases. A higher perforation rate leads to a shift of resonant peak towards higher frequencies. Besides, better acoustic performance could be obtained with the perforation being properly designed. Reducing the inlet/outlet radius can obviously improve the transmission loss without changing the frequency of resonant peak. The theories and conclusions in this study can be used for the design and optimization of resonators in various engineering applications.

1. Introduction

Recently, research on traditional silencers (expansion chamber muffler [1], quarter wavelength tube [2], concentric perforated resonator [3], etc.) has been continuously addressed. However, the research on resonators with perforated intruding inlets (PII) which could distinctly improve the acoustic performance has been neglected. As a promising kind of silencer element, a resonator with PII has the advantages of a compact structure and a desirable sound attenuation performance especially at mid and high frequencies [4]. Compared to the extended-tube resonator, additional perforations can effectively adjust and probably widen the frequency range of sound attenuation. Considering the design and engineering application of resonators with PII, it is significant to develop analytical approaches applied in the prediction for the transmission loss (TL).

The transfer matrix method [5] (TMM) based on plane wave theory is to obtain the four-pole parameters of a resonator, which are used to determine the TL. Chiu [6] used a one-dimensional (1D) TMM to calculate the TL of a muffler with perforated intruding inlet. In addition, with the effect of higher order modes excluded, the 1D approach is limited to the cut-off frequencies of plane wave [7]. Finite element method (FEM) takes more geometry details and three-dimensional effects into account [8], hence it can predict the acoustic performance more precisely. However, the model design and calculation process are time-consuming. It is also inconvenient to optimize the structure parameters if the acoustic performance is not satisfying. Therefore, apart from the 1D TMM, it is also necessary to develop a theoretical method, which is simultaneously accurate and efficient to calculate the TL of resonators with PII.

A two-dimensional (2D) method is applicable to calculate the TL for axisymmetric resonators. Selamet [9,10] predicted the TLs of both a single-chamber and a dual-chamber circular expansion muffler with extended inlet/outlet using a 2D weighted-integration method. However, the acoustic continuity equations to be solved in the approach will be complicated when many chambers are connected, since the transfer matrixes of the silencer elements are not considered and all continuity equations must be solved at one time. In recent years, the 2D approach was mostly applied to dissipative mufflers with single chambers [10–12]. Until

* Corresponding author at: Clean Energy Automotive Engineering Center, Tongji University, China.
E-mail address: guorong@tongji.edu.cn (R. Guo).

http://dx.doi.org/10.1016/j.apacoust.2016.09.012
0003-682X/

Nomenclature

S_n	modal amplitudes in region S (A, B, C, D, E)	L	total length of resonator chamber
c	sound speed in air	P	acoustic pressure
hd	diameter of the perforations	r_1	radius of the inlet tube
ht	thickness of the inner tube	r_2	radius of the outlet tube
d_1	diameter of the inlet tube	R	radius of the chambers
d_2	diameter of the outlet tube	T	transfer matrix
D_o	diameter of the chambers	U	particle velocity
f	frequency	v	air viscosity
J_0, J_1	Bessel functions of the first kind of order 0 and 1	x, x_1, x_2, x_3	axial coordinates
k_0	sound wave number in air	Y_0, Y_1	Bessel functions of the second kind of order 0 and 1
$k_{x,S,n}$	axial wave number in region S (A, B, C, D, E)	α	end correction coefficient
$k_{r,S,n}$	radial wave number in region S (A, B, C, D, E)	ζ	perforation impedance
li	length of inlet extension	σ	porosity
lm	length of perforation area	ρ	air density
lo	length of expansion chamber	$\varnothing_S^n(r)$	eigenfunctions in region S (A, B, C, D, E)

now, an effective 2D analytical method for TL calculation of resonators with PII has not been developed yet. Besides, the transfer matrix of the resonator, which is commonly used in the TL prediction of multi-chamber silencers [14], has not been derived through 2D approach.

The objective of the present work is to investigate the acoustic modeling of a resonator with PII, which has the advantages of a compact structure and a superior acoustic performance. Firstly, referring to an existing study, a 1D TMM without considering the mean flow is derived. In order to predict the acoustic performance more precisely, a 2D analytical method using direct integration is developed to calculate the pressure magnitudes for incident and reflected waves in the resonator, which are subsequently used to determine the four pole parameters of the transfer matrix. The applicability of the two TMMs is discussed in details through the comparisons to FEM and tests. To further study the characteristics of the resonator with PII, five groups of resonators are selected to evaluate the effects of structure parameters to the TL based on the 2D approach, including the length of perforated/non-perforated inlet extension, perforation rate and inlet/outlet radius.

2. Analytical methods

2.1. One-dimensional transfer matrix method

A resonator with PII consists of four kinds of acoustic propagation sections as shown in Fig. 1, including

(1) Straight tube, namely from point 1 to point 2 and from point 6 to point 7.
(2) Concentric perforated tube, namely from point 2, 3 to point 4, 5.

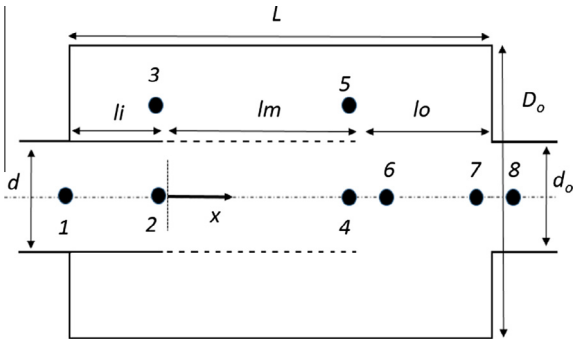

Fig. 1. The configuration and acoustic points of a resonator with PII.

(3) Sudden expansion at the open-ended inlet, namely from point 4, 5 to point 6.
(4) Sudden retraction at the outlet, namely from point 7 to point 8.

The total chamber length L is divided into an extended inlet of length li, a perforated tube of length lm, and an expansion chamber of length lo. Diameters of the inlet, outlet, and outer chamber are d, d_o, and D_o. The 1D TMM is to calculate the total transfer matrix of the resonator through multiplying transfer matrixes of every connected acoustic sections. The transfer matrixes for the straight tubes can be expressed as

$$\begin{bmatrix} p(1) \\ \rho cu(1) \end{bmatrix} = \begin{bmatrix} \cos(k_0 li) & j\sin(k_0 li) \\ j\sin(k_0 li) & \cos(k_0 li) \end{bmatrix} \begin{bmatrix} p(2) \\ \rho cu(2) \end{bmatrix} = [T1] \begin{bmatrix} p(2) \\ \rho cu(2) \end{bmatrix} \tag{1}$$

$$\begin{bmatrix} p(6) \\ \rho cu(6) \end{bmatrix} = \begin{bmatrix} \cos(k_0 lo) & j\sin(k_0 lo) \\ j\sin(k_0 lo) & \cos(k_0 lo) \end{bmatrix} \begin{bmatrix} p(7) \\ \rho cu(7) \end{bmatrix} = [T4] \begin{bmatrix} p(7) \\ \rho cu(7) \end{bmatrix} \tag{2}$$

where p is the sound pressure; ρ is the air density; c is the sound speed in air; u is the particle velocity; $k_0 = 2\pi/f$ is the sound wave number in air; f is the sound frequency. For the perforated region, the wave propagation functions in the inner tube and outer chamber are [15]

$$\begin{cases} \frac{\partial^2 p_i}{\partial x^2} - \left(\frac{4jk_0}{d\xi} - k_0^2\right) p_i + \frac{4jk_0}{d\xi} p_o = 0 \\ \frac{\partial^2 p_o}{\partial x^2} - \left(\frac{4jdk_0}{(D_o^2 - d^2)\xi} - k_0^2\right) p_o + \frac{4jdk_0}{(D_o^2 - d^2)\xi} p_i = 0 \end{cases} \tag{3}$$

where p_i, p_o, u_i and u_o are respectively the sound pressure and particle velocity of the inner tube and outer chamber; ξ (see Appendix A) is the acoustical impedance of the perforated tube. Eq. (3) can be written as a state function

$$\begin{bmatrix} p_i' \\ p_o' \\ p_i \\ p_o \end{bmatrix}' = [T] \begin{bmatrix} p_i' \\ p_o' \\ p_i \\ p_o \end{bmatrix} \tag{4}$$

The related solution can then be written as

$$\begin{bmatrix} p_i' \\ p_o' \\ p_i \\ p_o \end{bmatrix} = [\psi][C_1 e^{\lambda_1 x}, C_2 e^{\lambda_2 x}, C_3 e^{\lambda_3 x}, C_4 e^{\lambda_4 x}]^T \tag{5}$$

$[\psi]$ is the eigen matrix formed by four sets of eigen vectors of $[\boldsymbol{T}]$. Given that

$$\begin{cases} j\rho ck u_i = -p_i' \\ j\rho ck u_o = -p_o' \end{cases} \tag{6}$$

Substituting Eq. (6) into (5) yields

$$\begin{bmatrix} p_i \\ p_o \\ \rho c u_i \\ \rho c u_o \end{bmatrix} = [D_1(x)_{4\times 4}] \begin{Bmatrix} C_1 \\ C_2 \\ C_3 \\ C_4 \end{Bmatrix} \tag{7}$$

Substituting $x = 0$ and $x = lm$ into Eq. (7) and doing arrangement yield

$$\begin{bmatrix} p_2 \\ p_3 \\ \rho c u_2 \\ \rho c u_3 \end{bmatrix} = [T2] \begin{bmatrix} p_4 \\ p_5 \\ \rho c u_4 \\ \rho c u_5 \end{bmatrix} \tag{8}$$

The continuity equations between point 4, 5 and 6 without considering the mean flow can be described as [16]

$$\begin{cases} p_4 = p_6 \\ \rho c u_4 S_1 + \rho c u_5 S_2 = \rho c u_6 S_3 \\ S_1 p_4 + S_2 p_5 = S_3 p_6 \end{cases} \tag{9}$$

where $S_1 = \pi d^2/4$ is the area of the inner tube at the inlet; $S_2 = \pi (D_o{}^2 - d^2)/4$ is the area of the outer chamber at the inlet; $S_3 = \pi D_o{}^2/4$ is the area of the whole chamber. Considering the boundary condition at point 3, which is

$$\rho c u_3 / p_3 = -j \tan(k_0 li) = a \tag{10}$$

Assuming that

$$t = (a \cdot [T2]_{21} - [T2]_{41}, a \cdot [T2]_{22} - [T2]_{42}, a \cdot [T2]_{23} - [T2]_{43}, a \cdot [T2]_{24} - [T2]_{44}) \tag{11}$$

Substituting Eq. (10) into Eq. (8) and combing Eq. (11) yield

$$t \cdot (p_4, p_5, \rho c u_4, \rho c u_5)^T = 0 \tag{12}$$

Using Eqs. (9) and (12), the relationship between point 4, 5, and 6 can be written as

$$\begin{bmatrix} 1 & 0 & 0 & 0 \\ 0 & 0 & S_1 & S_2 \\ S_1 & S_2 & 0 & 0 \\ & t & & \end{bmatrix} \begin{bmatrix} p_4 \\ p_5 \\ \rho c u_4 \\ \rho c u_5 \end{bmatrix} = \begin{bmatrix} 1 & 0 \\ 0 & S_3 \\ S_3 & 0 \\ 0 & 0 \end{bmatrix} \begin{bmatrix} p_6 \\ \rho c u_6 \end{bmatrix} \tag{13}$$

Rearranging Eq. (13) yields

$$\begin{bmatrix} p_4 \\ p_5 \\ \rho c u_4 \\ \rho c u_5 \end{bmatrix} = [T3] \begin{bmatrix} p_6 \\ \rho c u_6 \end{bmatrix} \tag{14}$$

The transfer matrix of the sudden retraction section from point 7–8 can be written as

$$\begin{bmatrix} p_7 \\ \rho c u_7 \end{bmatrix} = \begin{bmatrix} 1 & 0 \\ 0 & S_4/S_3 \end{bmatrix} \begin{bmatrix} p_8 \\ \rho c u_8 \end{bmatrix} = [T5] \begin{bmatrix} p_8 \\ \rho c u_8 \end{bmatrix} \tag{15}$$

where S_4 is the area of the outlet tube. Thus, the transfer matrix from points 2, 3 to point 8 is

$$[To] = [T2][T3][T4][T5] \tag{16}$$

where $[\boldsymbol{To}]$ is a 4×2 matrix, and the relationship between point 1 and 8 can be written as:

$$\begin{bmatrix} p_1 \\ \rho c u_1 \end{bmatrix} = [T1] \begin{bmatrix} To_{11} & To_{12} \\ To_{31} & To_{31} \end{bmatrix} \begin{bmatrix} p_8 \\ \rho c u_8 \end{bmatrix} = [Tt] \begin{bmatrix} p_8 \\ \rho c u_8 \end{bmatrix} \tag{17}$$

Thus, the TL of a resonator with PII is

$$TL_1 = 20\log_{10}\left(\frac{d}{d_o}\frac{1}{2}|Tt_{11} + Tt_{12} + Tt_{21} + Tt_{22}|\right) \tag{18}$$

2.2. Two-dimensional transfer matrix method

As shown in Fig. 2, a resonator with PII can be divided into five sections: inlet *A*, extended inlet chamber *B*, perforated tube *C*, expansion chamber *D* and outlet *E*. Radiuses of the inlet tube, outlet tube and outer chamber are respectively r_1, r_2 and R.

The Helmholtz equation of sound wave in axisymmetric tube is expressed as [5]

$$\begin{cases} \frac{\partial^2 P}{\partial r^2} + \frac{1}{r}\frac{\partial P}{\partial r} + \frac{\partial^2 P}{\partial x^2} + k_0^2 P = 0 \\ k_0 = \omega/c = 2\pi f/c \end{cases} \tag{19}$$

where P is the sound pressure; k_0 is the wave number in air; f is the sound frequency; c is the sound velocity in air; r is the distance to the axis. Upon making use of the separation method of variables, the sound pressure is assumed as

$$P(r,x) = \sum_n R_n(r) X_n(x) \tag{20}$$

Then, Eq. (19) can be divided into two independent wave equations

$$\begin{cases} \frac{d^2 X(x)}{dx^2} = -k_x^2 X(x) \\ \frac{d^2 R(r)}{dr^2} + \frac{1}{r}\frac{dR(r)}{dr} + k_r^2 R(r) = 0 \end{cases} \tag{21}$$

Solutions of Eq. (21) is expressed as

$$\begin{cases} X_n(x) = S_n^+ e^{-jk_{x,S,n}x} + S_n^- e^{jk_{x,S,n}x} \\ R_n(r) = \phi_S^n(r) \end{cases} \tag{22}$$

Substituting Eq. (22) to Eq. (20) yields

$$P_S = \sum_{n=0}^{\infty} (S_n^+ e^{-jk_{x,S,n}x_S} + S_n^- e^{jk_{x,S,n}x_S}) \phi_S^n(r) \tag{23}$$

Combing the linear momentum equation, the axial particle velocity is derived as

$$U_{x,S} = \frac{j}{\rho\omega}\frac{\partial P_S}{\partial x} = \frac{1}{\rho\omega}\sum_{n=0}^{\infty} k_{x,S,n}(S_n^+ e^{-jk_{x,S,n}x_S} - S_n^- e^{jk_{x,S,n}x_S}) \phi_S^n(r) \tag{24}$$

where S stands for the five sections *A*, *B*, *C*, *D*, and *E*; S_n^+, S_n^- are the nth modal amplitudes corresponding to positive and negative x directions; $\varnothing_S^n(r)$ is the eigenfunction; $k_{r,S,n}$ is the nth radial wave

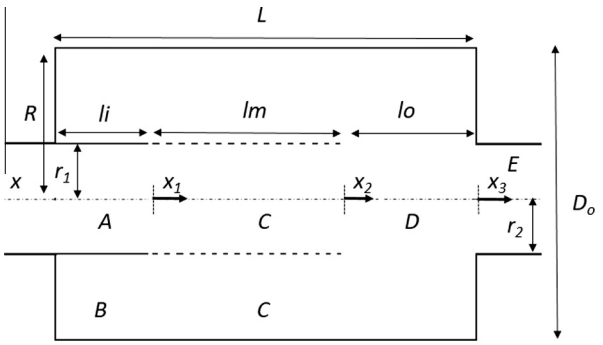

Fig. 2. The configuration and acoustic sections of a resonator with PII.

number; $k_{x,S,n}$ is the nth axial wave number. For section A, D and E with straight tubes, the eigenfunctions are [9]

$$\begin{cases} \phi_A^n(r) = J_0(k_{r,A,n}r) \\ \phi_D^n(r) = J_0(k_{r,D,n}r) \\ \phi_E^n(r) = J_0(k_{r,E,n}r) \end{cases} \tag{25}$$

For section B with a concentric annular tube, the eigenfunction is

$$\phi_B^n(r) = J_0(k_{r,B,n}r) - [J_1(k_{r,B,n}R)/Y_1(k_{r,B,n}R)]Y_0(k_{r,B,n}r) \tag{26}$$

For section C with concentric perforated tube, the eigenfunction is [11]

$$\phi_C^n(r) = \begin{cases} J_0(k_{r,C,n}r), 0 < r < r_1 \\ C_5\{J_0(k_{r,C,n}r) - [J_1(k_{r,C,n}R)/Y_1(k_{r,C,n}R)]Y_0(k_{r,C,n}r)\}, r_1 < r < R \end{cases} \tag{27}$$

With

$$C_5 = \frac{J_0(k_{r,C,n}r_1) + j\zeta(k_{r,C,n}/k_0)J_1(k_{r,C,n}r_1)}{J_0(k_{r,C,n}r_1) - [J_1(k_{r,C,n}R)/Y_1(k_{r,C,n}R)]Y_0(k_{r,C,n}r_1)} \tag{28}$$

where J_0 and J_1 are the zeroth and first order Bessel function of the first kind; Y_0 and Y_1 are the zeroth and first order Bessel function of the second kind. The relation between radial and axial wave numbers can be expressed as

$$k_{r,S,n}^2 + k_{x,S,n}^2 = k_0^2 \tag{29}$$

With $k_{r,A,n}$, $k_{r,B,n}$, $k_{r,D,n}$, $k_{r,E,n}$ being the solutions of Eigen functions satisfying

$$J_1(k_{r,A,n}r_1) = 0 \tag{30}$$

$$J_1(k_{r,B,n}r_1) - [J_1(k_{r,B,n}R)/Y_1(k_{r,B,n}R)]Y_1(k_{r,B,n}r_1) = 0 \tag{31}$$

$$J_1(k_{r,A,n}R) = 0 \tag{32}$$

$$J_1(k_{r,E,n}r_2) = 0 \tag{33}$$

The difference of the sound pressure across the perforated pipe ($r = r_1$) yields

$$P_{CI} - P_{CO} = \rho c\zeta U_{CI}, \ (r = r_1) \tag{34}$$

where ζ is the perforate acoustic impedance, which relates the sound pressure of the inner and outer section through the perforation interface (see Appendix A). P_{CI} and P_{CO} are respectively the sound pressure in the inner pipe and outer chamber of acoustic region C. U_{CI} is the particle velocity in the inner pipe. Combining Eqs. (23), (24), (27) and (34), the boundary condition for the solution of $k_{r,C,n}$ can be derived as

$$\frac{J_0(k_{r,C,n}r_1)}{J_1(k_{r,C,n}r_1)} + j\zeta\frac{k_{r,C,n}}{k_0} = \frac{J_0(k_{r,C,n}r_1)Y_1(k_{r,C,n}R) - Y_0(k_{r,C,n}r_1)J_1(k_{r,C,n}R)}{J_1(k_{r,C,n}r_1)Y_1(k_{r,C,n}R) - Y_1(k_{r,C,n}r_1)J_1(k_{r,C,n}R)} \tag{35}$$

At the interfaces AC, BC, CD and DE, the sound pressure and particle velocity have the boundary conditions as follows

$$P_A|_{x_1=0} = P_C|_{x_1=0}, (0 \leqslant r \leqslant r_1) \tag{36a}$$

$$P_B|_{x_1=0} = P_C|_{x_1=0}, (r_1 \leqslant r \leqslant R) \tag{36b}$$

$$P_D|_{x_2=0} = P_C|_{x_1=lm}, (0 \leqslant r \leqslant R) \tag{36c}$$

$$P_D|_{x_2=lo} = P_E|_{x_3=0}, (0 \leqslant r \leqslant r_2) \tag{36d}$$

$$U_{x,C}|_{x_1=0} = \begin{cases} U_{x,A}|_{x_1=0}, (0 \leqslant r \leqslant r_1) \\ U_{x,B}|_{x_1=0}, (r_1 \leqslant r \leqslant R) \end{cases} \tag{36e}$$

$$U_{x,C}|_{x_1=lm} = U_{x,D}|_{x_2=0}, (0 \leqslant r \leqslant R) \tag{36f}$$

$$U_{x,D}|_{x_2=lo} = \begin{cases} U_{x,E}|_{x_3=0}, (0 \leqslant r \leqslant r_2) \\ 0, (r_2 < r < R) \end{cases} \tag{36g}$$

With the sound pressure and particle velocity given by Eqs. (23) and (24), Eq. (36) yields

$$\sum_{n=0}^{N}(A_n^+ + A_n^-)\phi_{A,n}(r) = \sum_{n=0}^{N}(C_n^+ + C_n^-)\phi_{C,n}(r), (0 \leqslant r \leqslant r_1) \tag{37a}$$

$$\sum_{n=0}^{N}(B_n^+ + B_n^-)\phi_{B,n}(r) = \sum_{n=0}^{N}(C_n^+ + C_n^-)\phi_{C,n}(r), (r_1 \leqslant r \leqslant R) \tag{37b}$$

$$\sum_{n=0}^{N}(D_n^+ + D_n^-)\phi_{D,n}(r) = \sum_{n=0}^{N}(C_n^+ e^{-jk_{x,C,n}lm} + C_n^- e^{jk_{x,C,n}lm})\phi_{C,n}(r), (0 \leqslant r \leqslant R) \tag{37c}$$

$$\sum_{n=0}^{N}(D_n^+ e^{-jk_{x,D,n}lo} + D_n^- e^{jk_{x,D,n}lo})\phi_{D,n}(r) = \sum_{n=0}^{N}(E_n^+ + E_n^-)\phi_{E,n}(r), (0 \leqslant r \leqslant r_2) \tag{37d}$$

$$\sum_{n=0}^{N}k_{x,C,n}(C_n^+ - C_n^-)\phi_{C,n}(r) = \begin{cases} \sum_{n=0}^{N}k_{x,A,n}(A_n^+ - A_n^-)\phi_{A,n}(r), (0 \leqslant r \leqslant r_1) \\ \sum_{n=0}^{N}k_{x,B,n}(B_n^+ - B_n^-)\phi_{B,n}(r), (r_1 \leqslant r \leqslant R) \end{cases} \tag{37e}$$

$$\sum_{n=0}^{N}k_{x,C,n}(C_n^+ e^{-jk_{x,C,n}lm} - C_n^- e^{jk_{x,C,n}lm})\phi_{C,n}(r) = \sum_{n=0}^{N}k_{x,D,n}(D_n^+ - D_n^-)\phi_{D,n}(r), (0 \leqslant r \leqslant R) \tag{37f}$$

$$\sum_{n=0}^{N}k_{x,D,n}(D_n^+ e^{-jk_{x,D,n}lo} - D_n^- e^{jk_{x,D,n}lo})\phi_{D,n}(r) = \begin{cases} \sum_{n=0}^{N}k_{x,E,n}(E_n^+ - E_n^-)\phi_{E,n}(r), (0 \leqslant r \leqslant r_2) \\ 0 \end{cases} \tag{37g}$$

In order to solve Eq. (37), the infinite series of unknown amplitudes need to be truncated to a suitable number. Multiplying both sides of Eq. (37) by rdr gives

$$\sum_{n=0}^{N}(A_n^+ + A_n^-)\int_0^{r_{m,p1}}\phi_{A,n}(r)rdr = \sum_{n=0}^{N}(C_n^+ + C_n^-)\int_0^{r_{m,p1}}\phi_{C,n}(r)rdr \tag{38a}$$

$$\sum_{n=0}^{N}(B_n^+ + B_n^-)\int_{r_1}^{r_{m,p2}}\phi_{B,n}(r)rdr = \sum_{n=0}^{N}(C_n^+ + C_n^-)\int_{r_1}^{r_{m,p2}}\phi_{C,n}(r)rdr \tag{38b}$$

$$\sum_{n=0}^{N}(D_n^+ + D_n^-)\int_0^{r_{m,p3}}\phi_{D,n}(r)rdr = \sum_{n=0}^{N}(C_n^+ e^{-jk_{x,C,n}lm} + C_n^- e^{jk_{x,C,n}lm})\int_0^{r_{m,p3}}\phi_{C,n}(r)rdr \tag{38c}$$

$$\sum_{n=0}^{N}(E_n^+ + E_n^-)\int_0^{r_{m,p4}}\phi_{E,n}(r)rdr = \sum_{n=0}^{N}(D_n^+ e^{-jk_{x,D,n}lo} + D_n^- e^{jk_{x,D,n}lo})\int_0^{r_{m,p4}}\phi_{D,n}(r)rdr \tag{38d}$$

$$\sum_{n=0}^{N} k_{x,C,n}(C_n^+ - C_n^-)\int_0^{r_{m,U1}} \phi_{C,n}(r)rdr = \begin{cases} \sum_{n=0}^{N} k_{x,A,n}(A_n^+ - A_n^-)\int_0^{r_{m,U1}} \phi_{A,n}(r)rdr, (0 \leqslant r_{m,U1} \leqslant r_1) \\ \sum_{n=0}^{N} k_{x,A,n}(A_n^+ - A_n^-)\int_0^{r_1} \phi_{A,n}(r)rdr + \sum_{n=0}^{N} k_{x,B,n}(B_n^+ - B_n^-)\int_{r_1}^{r_{m,U1}} \phi_{B,n}(r)rdr, (r_1 \leqslant r_{m,U1} \leqslant R) \end{cases} \tag{38e}$$

$$\sum_{n=0}^{N} k_{x,C,n}(C_n^+ e^{-jk_{x,C,n}lm} - C_n^- e^{jk_{x,C,n}lm})\int_0^{r_{m,U}} \phi_{C,n}(r)rdr = \sum_{n=0}^{N} k_{x,D,n}(D_n^+ - D_n^-)\int_0^{r_{m,U}} \phi_{D,n}(r)rdr \tag{38f}$$

$$\sum_{n=0}^{N} k_{x,D,n}(D_n^+ e^{-jk_{x,D,n}lo} - D_n^- e^{jk_{x,D,n}lo})\int_0^{r_{m,U}} \phi_{D,n}(r)rdr = \begin{cases} \sum_{n=0}^{N} k_{x,E,n}(E_n^+ - E_n^-)\int_0^{r_{m,U}} \phi_{E,n}(r)rdr, (0 \leqslant r_{m,U} \leqslant r_2) \\ \sum_{n=0}^{N} k_{x,E,n}(E_n^+ - E_n^-)\int_0^{r_2} \phi_{E,n}(r)rdr, (r_2 \leqslant r_{m,U} \leqslant R) \end{cases} \tag{38g}$$

With

$$\begin{cases} r_{m,P1} = \frac{m}{N+1} r_1, m = 1, \ldots, N+1 \\ r_{m,P2} = r_1 + \frac{m}{N+1}(R - r_1), m = 1, \ldots, N+1 \\ r_{m,P4} = \frac{m}{N+1} r_2, m = 1, \ldots, N+1 \\ r_{m,P3} = r_{m,U} = \frac{m}{N+1} R, m = 1, \ldots, N+1 \end{cases} \tag{39}$$

The simplification of Eq. (38) can refer to Appendix B. Using the rigid boundary conditions in section B at $x = -li$, the relation between the positive and negative modal amplitudes is

$$B_n^+ = B_n^- e^{-2jk_{x,B,n}li} \tag{40}$$

In 2D analytical method, waves in the inlet/outlet can be assumed as planar, which means an acoustic transfer matrix can be acquired between the inlet and outlet

$$\begin{bmatrix} P_A \\ \rho c U_A \end{bmatrix} = \begin{bmatrix} T_{11} & T_{12} \\ T_{21} & T_{22} \end{bmatrix} \begin{bmatrix} P_E \\ \rho c U_E \end{bmatrix} \tag{41}$$

In order to determine the four-pole parameters of the transfer matrix, the incoming wave of the inlet is assumed as planar with $A_0^+ = 1$; $A^+_{1,2\ldots N} = 0$. Eq. (38) should be solved twice under two different outlet conditions

(1) Total reflection end with $E^-_{0,1\ldots N} = E^+_{0,1\ldots N}$.
(2) Anechoic end with $E^-_{0,1\ldots N} = 0$.

Eq. (38) gives 7(N + 1) relations for 7(N + 1) unknowns. For calculation convenience, assuming

$$X = [A_0^- \ldots A_N^-, B_0^- \ldots B_N^-, C_0^+ \ldots C_N^+, C_0^- \ldots C_N^-, D_0^+ \ldots D_N^+, D_0^- \ldots D_N^-, E_0^+ \ldots E_N^+] \tag{42}$$

Eq. (38) can be written as linear equations $\boldsymbol{a}X = \boldsymbol{b}$. Then the solutions can be obtained as $X = \boldsymbol{a}^{-1}\boldsymbol{b}$. With the first outlet condition, it can be determined that

$$Tm_{11} = \frac{p_A}{p_E} = \frac{1 + A_0^-}{2E_0^+}\bigg|_{E^-_{0,1,\ldots N} = E^+_{0,1,\ldots N}} \tag{43}$$

$$Tm_{21} = \frac{\rho c U_A}{p_E} = \frac{1 - A_0^-}{2E_0^+}\bigg|_{E^-_{0,1,\ldots N} = E^+_{0,1,\ldots N}} \tag{44}$$

With the second outlet condition, it can be derived that

$$Tm_{12} = \frac{p_A}{\rho c U_E} = \frac{1 + A_0^-}{E_0^+}\bigg|_{E^-_{0,1,\ldots N} = 0} - Tm_{11} \tag{45}$$

$$Tm_{22} = \frac{\rho c U_A}{\rho c U_E} = \frac{1 - A_0^-}{E_0^+}\bigg|_{E^-_{0,1,\ldots N} = 0} - Tm_{21} \tag{46}$$

Considering the extended inlet/outlet, the total transfer matrix can be written as

$$[TT] = \begin{bmatrix} \cos(k_0 li) & j\sin(k_0 li) \\ j\sin(k_0 li) & \cos(k_0 li) \end{bmatrix} \begin{bmatrix} Tm_{11} & Tm_{12} \\ Tm_{21} & Tm_{22} \end{bmatrix} \tag{47}$$

The TL of the resonator can be determined as

$$TL_2 = 20\log_{10}\left(\frac{r_1}{r_2}\frac{1}{2}|TT_{11} + TT_{12} + TT_{21} + TT_{22}|\right) \tag{48}$$

To solve the above equations, the infinite series of amplitudes need to be truncated to a suitable number. For the frequency range and geometry discussed in this study, the result is sufficiently accurate when $N > 5$ so that $N = 6$ is used in the remainder of the study.

3. Experimental validation and comparison

The two-load technique is applied in the TL measurement by means of an impedance tube, as shown in Fig. 3. The tests were carried out in the semi-anechoic room at Tongji University. The test facility consists of a LMS SCADAS III 306 data acquisition system, a full frequency band loudspeaker and four microphones. The sampling frequency in the test was 16,384 Hz. Based on the requirements for the outlet, the first condition of the outlet is an open end, and the other condition is an end, which is filled up with insulation cotton [3]. In order to determine the accuracies of the TMMs, two resonators which respectively has a chamber length of 90 mm and 50 mm are selected. The diameters of the chamber and inner tube are chosen according to usual engineering applications. For the configurations, the present study considers $D_0 = 90$ mm for the chamber diameter, $d = d_0 = 45$ mm for the inlet/outlet ducts, $hd = 3$ mm; $ht = 2$ mm; $\sigma = 12.68\%$ for parameters of the perforation.

For the resonator with long chamber, Fig. 4(a) compares the test results with TLs calculated by 1D TMM, 2D TMM, and FEM. The acoustic FEM simulation is implemented through a commercial simulation software LMS.virtual.lab, and the element numbers of the hexahedral meshes are respectively 53205 and 35805. The results of 1D and 2D TMM are respectively calculated by Eqs. (18) and (48). It can be seen that, although the 1D approach may be useful for an approximate estimation of the TL, there is still a minor frequency deviation between the calculation result of 1D TMM and test. Whereas TL calculated by 2D TMM matches well with that of FEM, and shows a good agreement with the test result. The amplitude discrepancy between prediction and test is assessed in relation to the inaccuracy of perforation impedance model and imperfection of the test set-up.

As for the resonator with short chamber, there is an obvious mismatch between the result of 1D approach and test as shown in Fig. 4(b). The primary reason is that a resonator with PII is similar to an extended-tube resonator. The end correction of inlet extension needs to be considered for 1D approach [17]. In the case of perforated inlet, such a general correlation is hard to be obtained, since there is no coupling between the quarter wave effect of the extension and the duct-cavity resonance of the perforated tube [18]. Kang and Ji [19] also found out that an approximate expression for the acoustic length correction of duct extension is not applicable to short chambers as the radial waves cannot be decayed sufficiently. In comparison, the 2D TMM is able

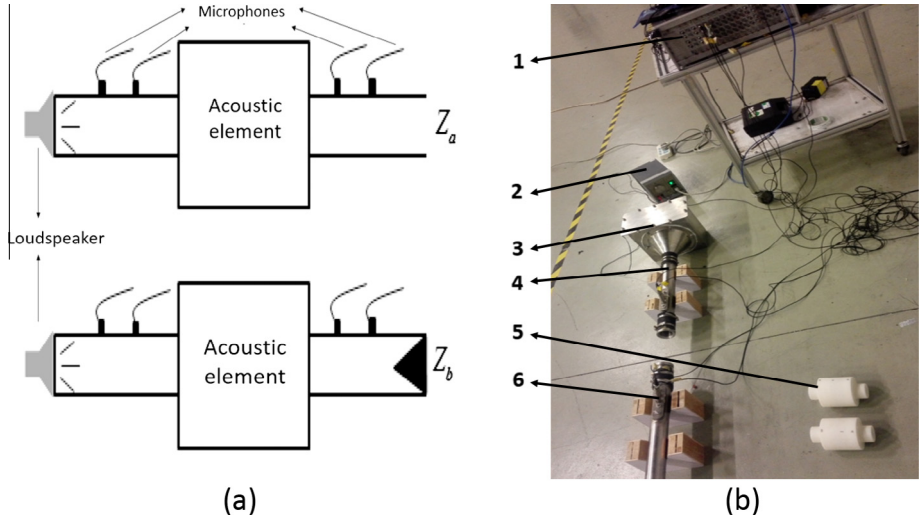

Fig. 3. Sketch of the TL test, (a) the test scheme, (b) the test set-up: 1. data acquisition system; 2. power amplifier; 3. loudspeaker; 4. impedance tube; 5. resonator; 6. Microphones.

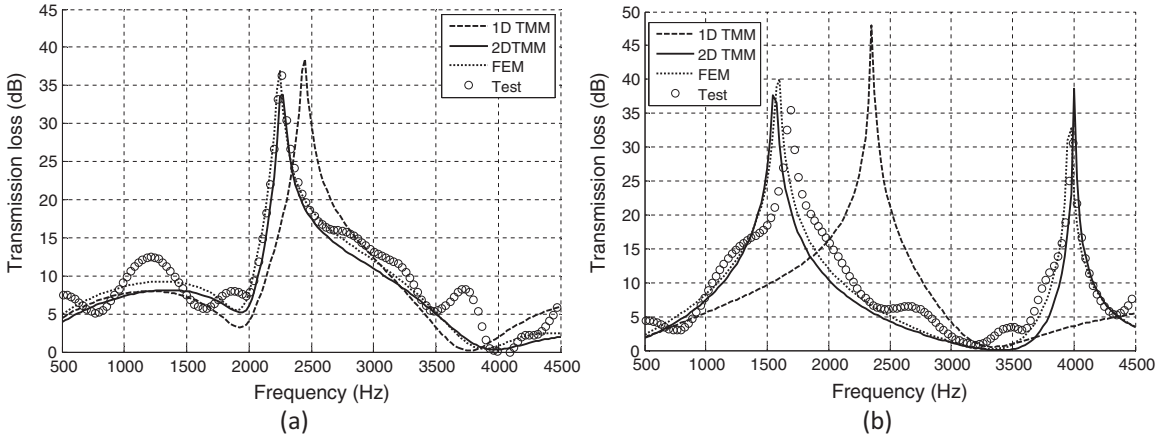

Fig. 4. TL comparison of resonators with PII (a) TL of the resonator with long chamber, li = 20 mm, lm = 30 mm, lo = 40 mm and (b) TL of the resonator with short chamber, li = 25 mm, lm = 15 mm, lo = 10 mm.

to calculate the TL precisely without considering the end corrections or the cut-off frequencies of resonator chambers. Besides, it is much more timesaving than FEM. Hence, the 2D TMM derived here is validated to be very accurate and efficient in calculating the TLs of resonators with PII.

4. Effects of structure parameters on TL

To further study the characteristics of the resonator with PII, five groups of geometries are selected to analyze the effect of structure parameters to the acoustic performance based on the 2D TMM. As shown in Table 1, referring to the resonator geometry discussed above, group 1–5 respectively has a varying parameter, which totally has 30 data points with a same interval. The expression [M:N] stands for a lower limit of M and a upper limit of N. The corresponding interval is $(N - M)/(30 - 1)$. The frequency step size for calculation is 10 Hz. The acoustic performance is expressed by three TL targets in the frequency range of 0–4000 Hz: the frequency of first resonant peak (Target A), the amplitude of highest dome (Target B) and the bandwidth (Target C) that the TL exceeds 20 dB which is commonly used to evaluate whether a resonator can effectively attenuate noises. Other parameters are the same with that of the resonators with PII in Section 3.

4.1. Effect of inlet extension and perforation tube

Fig. 5 shows the effect of the inlet extensions to the three acoustic targets through calculating TLs in group 1. As the length of inlet extension increases from 5 mm to 50 mm, the first resonance peak moves to a lower frequency range and the frequency deviation

Table 1
Groups of resonators with PII.

Group	r_1 (mm)	r_2 (mm)	li (mm)	lm (mm)	σ (%)
1	22.5	22.5	[5:50]	20	4
2	22.5	22.5	20	[5:50]	4
3	22.5	22.5	10	20	[1:10]
4	[16.5:30]	22.5	10	20	4
5	22.5	[16.5:30]	10	20	4

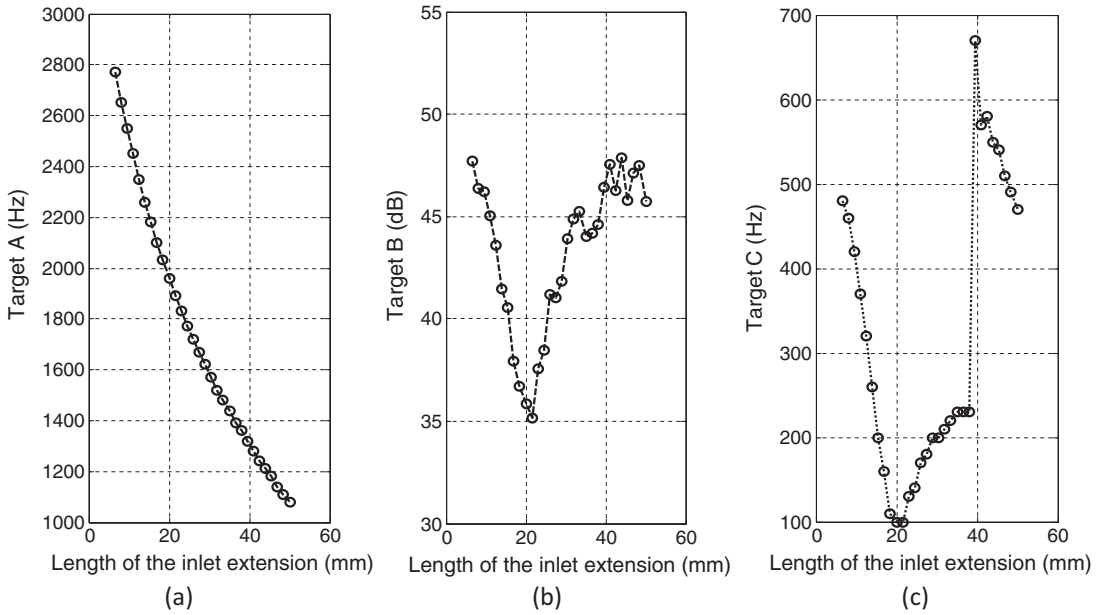

Fig. 5. Effects of the inlet extension length, (a) effect to Target A, (b) effect to Target B, and (c) effect to Target C.

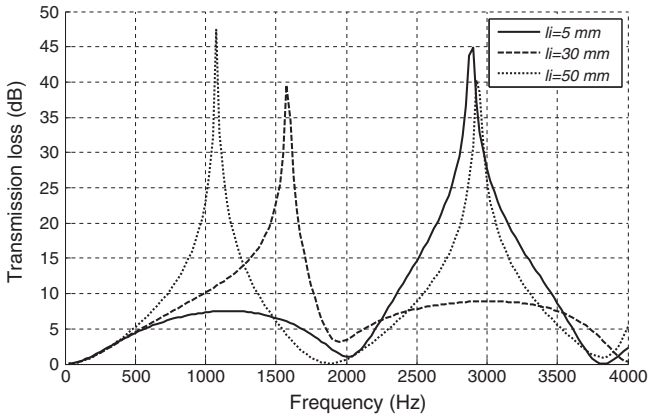

Fig. 6. TL of resonators with different length of inlet extensions.

reaches 1700 Hz. The reason is that the extended inlet can be seen as a quarter-wavelength tube whose resonant frequency is lowered when the tube gets longer. The maximum amplitude and the sound attenuation bandwidth decrease until they reach the minimum of 35 dB and 100 Hz while the length of inlet extension is 20 mm. This is resulted from the resonant frequency shift of the inlet tube, which makes the dome shift from a basic TL peak to a trough of the expansion chamber. Subsequently, these two target values are increased because the resonance dome of the inlet starts moving from the TL trough to another peak of the expansion chamber. The sound attenuation bandwidth sharply increases to 680 Hz and maintains a high value when the length of inlet exceeds 40 mm, while the maximum TL amplitude becomes stable. It is because that for a quarter-wavelength tube, the frequency interval between two resonant peaks is narrowed with the length of tube increasing. Hence, the TL exhibits more superposition of domes as illustrated in Fig. 6. The perforated tube has a similar feature

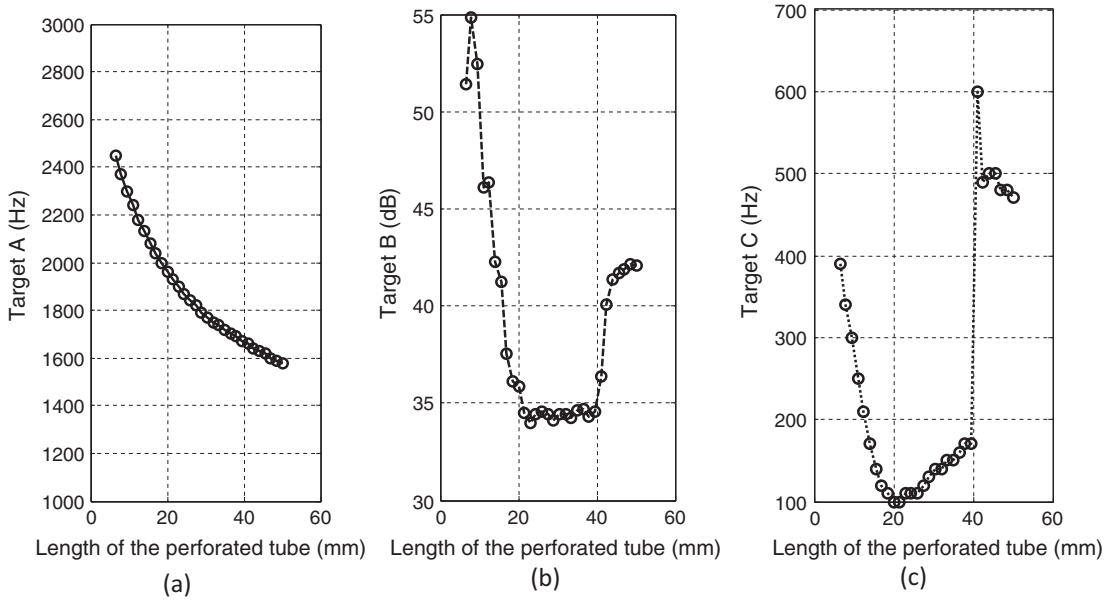

Fig. 7. Effects of the perforated tube length, (a) effect to Target A, (b) effect to Target B, and (c) effect to Target C.

of extended inlet so that as the length of perforated tube increases, the acoustic targets have the same change trends with that of the inlet extension. However, in Fig. 7, the first peak only reduces by 850 Hz due to the perforations although the length of perforated tube in group 2 has a same varying interval as that of the inlet extension in group 1.

4.2. Effect of perforation rate

To further study the effect of perforations, resonators with various perforation rates in group 3 are investigated and the changes of the acoustic targets are shown in Fig. 8. Apparently, the resonant peak moves to higher frequency range as the perforation rate increases. The maximum TL amplitude reduces by 4 dB, which is nearly negligible when the perforation rate increases to 10%, whereas the sound attenuation bandwidth rises by 200 Hz. It is because that a perforated element can be seen as a sort of Helmholtz resonator. The perforation holes are the neck, which connects the inner tube and resonant chamber. Therefore, the resonant frequency becomes higher as the cross-section area of the neck is enlarged by raising the perforation rate, and the resonance peak of the perforations is superposed on the base dome of expansion chamber, hence the sound attenuation bandwidth is widen, as shown in Fig. 9. When the perforation rate exceeds 10%, the maximum amplitude continues to drop slowly, while the bandwidth remains steady. Actually, reducing the length of inlet extension can lead to a similar result. However, the use of perforated tube can effectively lower the pressure drop of the resonator, which makes the resonator with PII a fine substitute for extended-tube resonator. By properly designing the perforation rate, an excellent acoustic attenuation performance can be obtained especially at mid and high frequencies.

4.3. Effect of inlet/outlet radius

As for the resonator with PII, the diameters of the inlet and outlet are unrelated so that they can be adjusted separately. Figs. 10 and 11 respectively show the effect of the inlet and outlet radiuses to the TL. Changing the radiuses has almost no effect on the frequency of first dome. However, the maximum TL amplitude increases and the sound attenuation bandwidth is obviously widen when the inlet or outlet radius becomes smaller. In fact, the effects

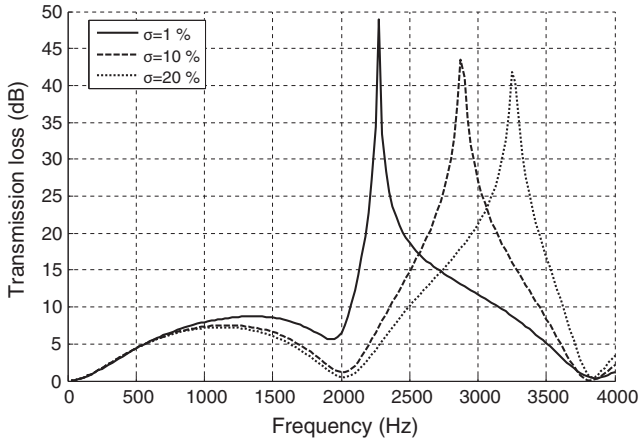

Fig. 9. TL of resonators with different perforation rate.

are similar to that of a simple expansion muffler. Decreasing the radius of inlet/outlet tube leads to an increase of expansion ratio, causing a higher TL peak and a wider sound attenuation bandwidth. The resonant frequency barely shifts because it is only influenced by the chamber length. It is also noted that, the variation of inlet radius has greater effects on Target B and Target C than that of outlet radius. The primary reason is that the perforated tube is connected to the inlet so that reducing inlet radius provides a bigger resonant chamber space for the perforation, which will also improve the acoustic performance. This certain feature can be utilized in the design and optimization of multi-chamber silencers conjugated with PII.

5. Conclusions

In this paper, both 1D and 2D approaches are applied to predict the acoustic performance of a resonator with PII. Based on a previous mathematical model, a 1D TMM without considering the mean flow is derived. However, through two groups of comparisons with tests, it is concluded that the applicability of 1D TMM is limited by the resonator geometry even when the frequency is below the cut-off value of plane wave. Obvious deviations will occur if the chamber length becomes short, and additional end corrections may be necessary. In comparison, TLs calculated by the 2D TMM, which

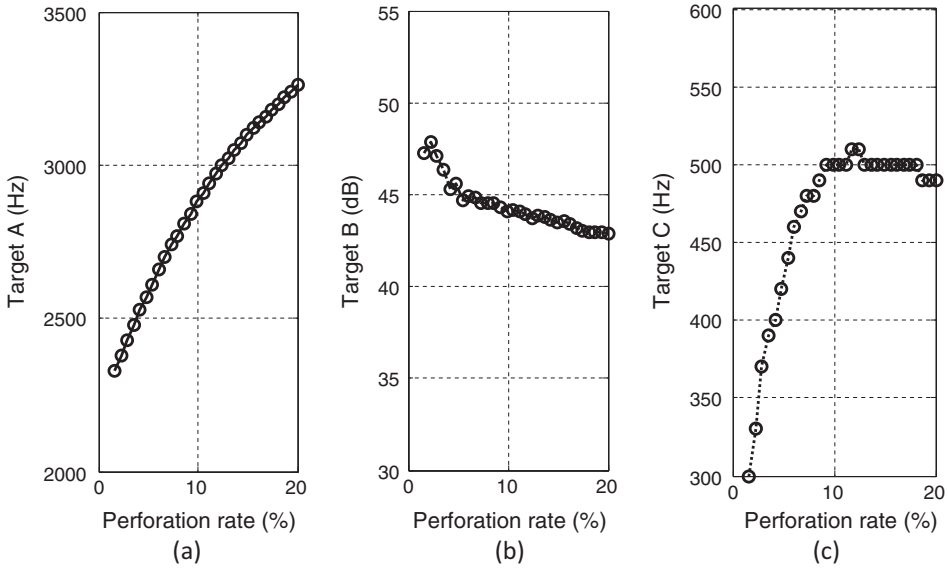

Fig. 8. Effects of the perforation rate, (a) effect to Target A, (b) effect to Target B, and (c) effect to Target C.

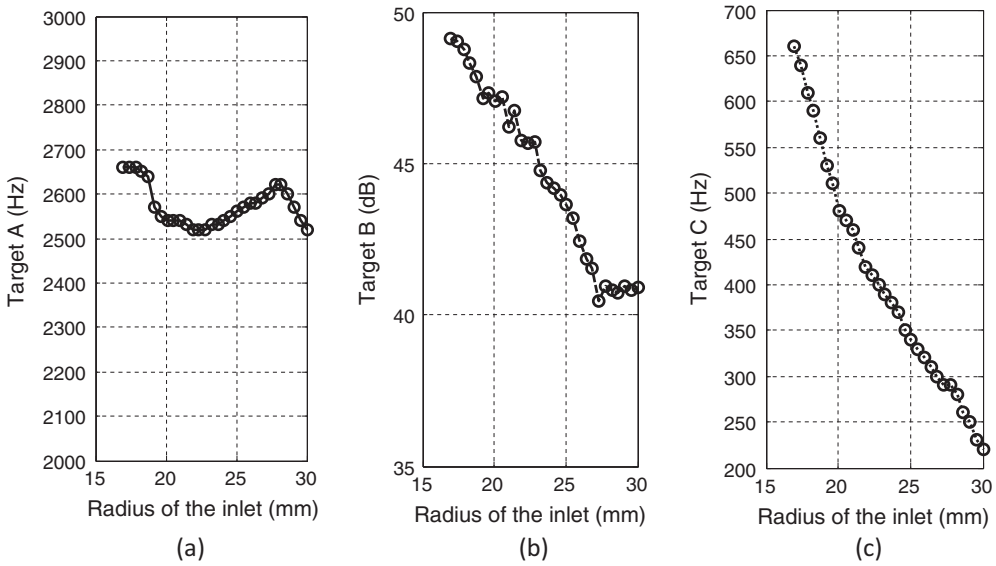

Fig. 10. Effects of the inlet radius, (a) effect to Target A, (b) effect to Target B, and (c) effect to Target C.

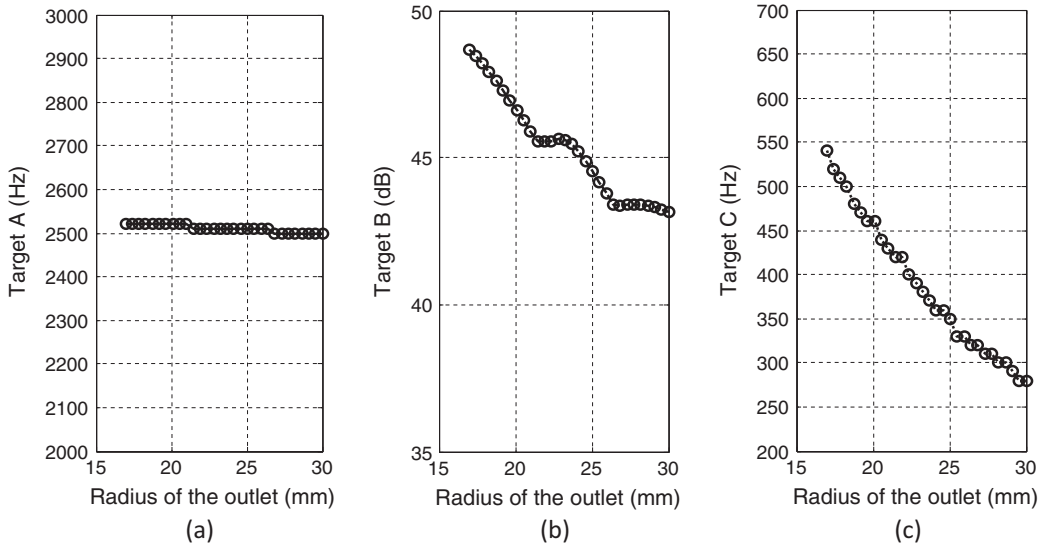

Fig. 11. Effects of the outlet radius, (a) effect to Target A, (b) effect to Target B, and (c) effect to Target C.

is as timesaving as 1D approach match well with that of FEM, and show a good agreement with the tests. Hence, the 2D approach developed in this study is validated to be very accurate and effective in calculating the TLs of resonators with PII.

In order to investigate the characteristics of the resonator with PII, three acoustic targets are defined to evaluate the effects of structure parameters to the TL of a resonator with PII based on the 2D approach. Through five groups of calculations, it is shown that the number of resonant peaks increases and the frequencies decrease as the length of perforated or non-perforated inlet extension is increased. As the perforation rate becomes higher, the resonant peaks shift to a higher frequency range and better acoustic performance could be obtained if the perforation is designed properly. The decrease of inlet/outlet radius provides higher TL amplitudes without influencing resonant frequencies. The theoretical methods and conclusions in this paper can be applied to the acoustic analysis and structure optimization for multi-chamber resonators conjugated with PII.

Acknowledgements

This research is supported by the Fundamental Research Funds for the Central Universities (2016). Authors gratefully acknowledge the resources provided by the Clean Energy Automotive Engineering Center of Tongji University.

Appendix A

The perforation impedance model applied in this study follows Ji's empirical expression as [20]

$$\zeta = (1/\sigma)(R_0 + jX_0) \tag{A.1}$$

With

$$\begin{cases} R_0 = (1 + ht/hd)\sqrt{8k_0\nu/\rho c} \\ X_0 = k_0(ht + \alpha hd) \end{cases} \tag{A.2}$$

where v is the kinetic viscosity of air; and α is the end correction coefficient of holes, expressed as

$$\alpha = \begin{cases} 0.85\left[1 - 2.34\left(\frac{\sigma}{\pi}\right)^{0.5}\right], & 0 < \left(\frac{\sigma}{\pi}\right)^{0.5} \leqslant 0.25 \\ 0.668\left[1 - 1.9\left(\frac{\sigma}{\pi}\right)^{0.5}\right], & 0.25 < \left(\frac{\sigma}{\pi}\right)^{0.5} \leqslant 0.5 \end{cases} \tag{A.3}$$

Appendix B

The integrals of Eqs. (37a)–(37g) can be analytically determined in light of [13]

For the zeroth-order Bessel function of the first kind,

$$\int_0^{r_0} J_0(\lambda r) r \, dr = \begin{cases} r_0^2/2 & \lambda = 0 \\ J_1(\lambda r_0) r_0/\lambda & \lambda \neq 0 \end{cases} \tag{B.1}$$

For the zeroth-order Bessel function of the second kind,

$$\int_0^{r_0} Y_0(\lambda r) r \, dr = r_0 Y_1(\lambda r_0)/\lambda + 2/(\pi\lambda^2) \tag{B.2}$$

References

[1] Banerjee S, Jacobi AM. Transmission loss analysis of single-inlet/double-outlet (SIDO) and double-inlet/single-outlet (DISO) circular chamber mufflers by using Green's function method. Appl Acoust 2013;74(12):1499–510.

[2] Howard CQ, Craig RA. Noise reduction using a quarter wave tube with different orifice geometries. Appl Acoust 2014;76(1):180–6.

[3] Guo R, Zhu W. Acoustic attenuation performance of a perforated resonator with a multi-chamber and its optimal design. Proc IMechE D J Auto Eng 2014;228(9):1051–60.

[4] Chang YC, Chiu MC. Shaped optimization of multi-chamber mufflers with open-ended perforated inlets using a genetic algorithm. Proc Meet Acoust Soc Am 2010;9(1):04003.

[5] Munjal ML. Acoustics of ducts and mufflers. New York: Wiley-Interscience publication; 2014. p. 74–83.

[6] Chiu MC. Optimal design of multi-chamber mufflers hybridized with perforated intruding inlets and resonating tubes using simulated annealing. J Vibrat Acoust 2010;132(5):1515–6.

[7] Gerges SNY, Jordan R, Thieme FA, Bento Coelho JL, Arenas JP. Muffler modeling by transfer matrix method and experimental verification. J Acoust Soc Am 2005;27(2):132–40.

[8] Mehdizadeh OZ, Paraschivoiu M. A three-dimensional finite element approach for predicting the transmission loss in mufflers and silencers with no mean flow. Appl Acoust 2005;66(8):902–18.

[9] Selamet A, Ji ZL. Acoustic attenuation performance of circular expansion chamber with extended inlet/outlet. J Sound Vib 1998;213(4):601–17.

[10] Selamet A, Denia FD, Besa AJ. Acoustic behavior of circular dual-chamber mufflers. J Sound Vib 2003;265(5):967–85.

[11] Selamet A, Xu MB, Lee IJ, Huff NT. Analytical approach for sound attenuation in perforated dissipative silencers. J Acoust Soc Am 2004;115(5):2091–9.

[12] Selamet A, Xu MB, Lee IJ, Huff NT. Analytical approach for sound attenuation in perforated dissipative silencers with inlet/outlet extensions. J Acoust Soc Am 2005;117(4):2091–9.

[13] Denia FD, Selamet A, Fuenmayor FJ, Kirby R. Acoustic attenuation performance of perforated dissipative mufflers with empty inlet/outlet extensions. J Sound Vib 2007;302(4):1000–17.

[14] Chiu MC, Chang YC. Numerical studies on venting system with multi-chamber perforated mufflers by GA optimization. Appl Acoust 2008;69(11):1017–37.

[15] Guo R, Tang W, Zhu W. Comparison of 1D transfer matrix method and finite element method with tests for acoustic performance of multi-chamber perforated resonator. Appl Acoust 2016;112:140–6.

[16] Chang YC, Chiu MC, Liu WC. Shape optimization of one-chamber mufflers with perforated intruding tubes using a simulated annealing method. J Mar Sci Technol 2010;18(4):597–610.

[17] Chaitanya P, Munjal ML. Effect of wall thickness on the end corrections of the extended inlet and outlet of a double-tuned expansion chamber. Appl Acoust 2011;72(1):65–70.

[18] Torregrosa AJ, Broatch A, Payri R, Gonzalez F. Numerical estimation of end corrections in extended-duct and perforated-duct mufflers. J Vibrat Acoust 1999;121(3):302–8.

[19] Kang ZX, Ji ZL. Acoustic length correction of duct extension into a cylindrical chamber. J Sound Vib 2008;310:782–91.

[20] Ji ZL. Boundary element acoustic analysis of hybrid expansion chamber silencer with perforated facing. Eng Anal Boundary Elem 2010;34(7):690–6.